Modeling of Seismic Wave Propagation at the Scale of the Earth on a Large Beowulf

[Extended Abstract]

Dimitri Komatitsch
Seismological Laboratory
California Institute of Technology
Pasadena, California 91125, USA
komatits@gps.caltech.edu

Jeroen Tromp
Seismological Laboratory
California Institute of Technology
Pasadena, California 91125, USA
jtromp@gps.caltech.edu

ABSTRACT

We use a parallel spectral-element method to simulate the propagation of seismic waves generated by earthquakes in the entire 3-D Earth. The method is implemented using MPI on a large PC cluster (Beowulf) with 151 processors and 76 Gb of RAM. It is based upon a weak formulation of the equations of motion and combines the flexibility of a finite-element method with the accuracy of a pseudospectral method. The finite-element mesh honors all discontinuities in the Earth velocity model. To maintain a relatively constant number of grid points per seismic wavelength, the size of the elements is increased with depth in a conforming fashion, thus retaining a diagonal mass matrix. The effects of attenuation and anisotropy are incorporated. We benchmark spectral-element synthetic seismograms against a normal-mode reference solution for a spherically symmetric Earth velocity model. The two methods are in excellent agreement for all waves with periods greater than 20 seconds.

1. INTRODUCTION

Modeling seismic wave propagation resulting from large earthquakes at the scale of the entire Earth using fully three-dimensional (3-D) velocity models poses a formidable numerical challenge. The effects of an anisotropic asthenosphere, a slow and very thin crust, sharp fluid-solid discontinuities at the inner-core (ICB) and core-mantle (CMB) boundaries, and attenuation must all be accounted for. In this article we demonstrate that the spectral-element method (SEM), introduced more than 15 years ago in computational fluid mechanics [12], can meet this challenge. We reach unprecedented resolution by using a message-passing algorithm on a large cluster of PCs (Beowulf) with 151 processors and 76 Gb of RAM.

The SEM has previously been used to accurately model wave propagation on local and regional scales [13, 8, 11]. Examples of such local or regional simulations include seismic risk assessment in sedimentary basins such as Los Angeles, Tokyo or Mexico City, and active seismic experiments in oil fields for the petroleum industry. It has also recently been applied to the problem of global wave propagation in innovative work by [5] and [4]. They use a so-called 'mortar' version of the SEM [1], which allows for non-conforming meshes. This makes mesh design more flexible, but comes at a significant increase in the complexity and cost of the implementation, because the mass matrix is no longer diagonal on the non-conforming interfaces, and as a result an iterative solver has to be used to solve the non-diagonal system. In this work we use a classical SEM based upon a conforming mesh that retains a diagonal mass matrix, thus greatly simplifying the algorithm and reaching high parallel efficiency, which in turn allows us to perform for the first time 3-D global simulations at unprecedented resolution. Compared to previous works, we introduce the effect of anisotropy of seismic velocities in the asthenosphere (the upper 220 km of the Earth in the upper mantle), and also incorporate the effect of attenuation of the waves (loss of energy due to anelastic behavior of the materials). In addition, we also employ a powerful way of handling the fluid region of the model (the fluid outer core of the Earth, which is in contact with the solid mantle and the solid inner core) based upon a simple and efficient domain decomposition technique.

2. DESIGNING A MESH FOR THE EARTH

As in any finite-element method, a first crucial step towards the accurate simulation of 3-D seismic wave propagation resulting from earthquakes is the design of a mesh. A classical spectral-element method (SEM) relies upon a mesh of hexahedral finite elements Ω_e that are isomorphous to the cube. Tetrahedra that are classical in finite element methods are excluded in the SEM because of the tensorisation of the polynomial basis that is required to obtain an exactly diagonal mass matrix, as will be explained in Section 3. The six sides of each hexahedral element must match up *exactly* with the sides of neighboring elements. Such a mesh is traditionally called a *geometrically conforming* mesh in the finite-element literature. For reasons of accuracy, a good mesh should honor all the major velocity discontinuities in the model, and the size of the elements should reflect the distribution of wave speeds, such that one maintains a relatively similar number of grid points per seismic wave-

SC2001 November 2001, Denver

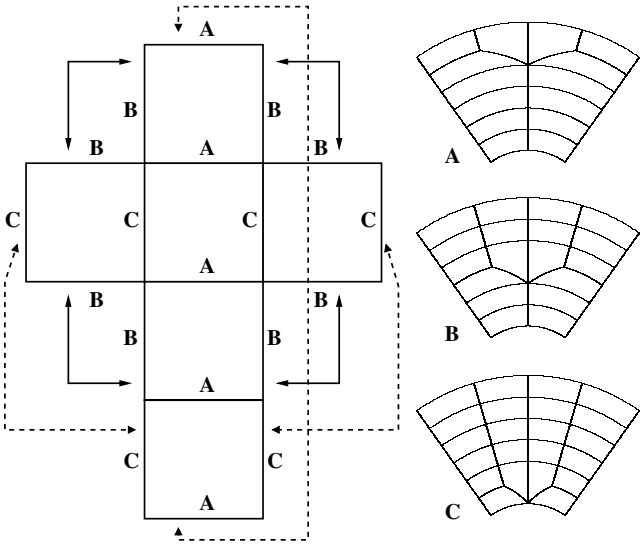

Figure 1: View of the six building blocks that constitute the cubed sphere. Analytical relations map each of the six faces of the cube to the surface of the sphere. Besides a top and bottom, each block has four sides that need to match up exactly with four other blocks to complete the cube, as indicated by the arrows. The mesh size also needs to be increased in the globe as a function of depth to maintain a similar number of grid points per wavelength throughout the model. This is accomplished in three stages; schematically, these four sides have one of three designs: A, B, or C, as illustrated on the right. When the six blocks are fitted together to make the entire globe, they match perfectly.

length throughout the model. Since wave speed generally increases with depth in the Earth, this implies that the elements should become gradually larger with depth. These requirements make the design of a good mesh for the globe challenging.

The mesh we use is based upon the concept of the quasi-uniform gnomonic projection, or 'cubed-sphere' [15, 17, 14] that was first introduced for seismic wave propagation problems by [5]. The key idea is to map each of the six sides of a cube to the surface of the sphere. An increase in element size, to adapt it to the variations of wave speed with depth, can be obtained by first doubling the mesh in one lateral direction, and, subsequently, at a greater depth, increasing its size in the other lateral dimension. Figure 1 illustrates how this may be accomplished for the entire globe based upon a three-stage doubling as a function of depth. Note that there are three types of chunks: AB, AC, and BC. In each of the types the doubling is performed at different levels, such that the final six chunks fit together perfectly to make the entire globe.

The final mesh used in the simulations is shown in Figure 2 and is designed to honor all velocity discontinuities in the spherically-symmetric 1-D standard reference wave velocity model for the Earth, which is called the Preliminary Reference Earth Model (PREM) [7]. Each of the six chunks has 240×240 elements at the free surface and, as a result of the three doublings with depth, 30×30 elements at the ICB.

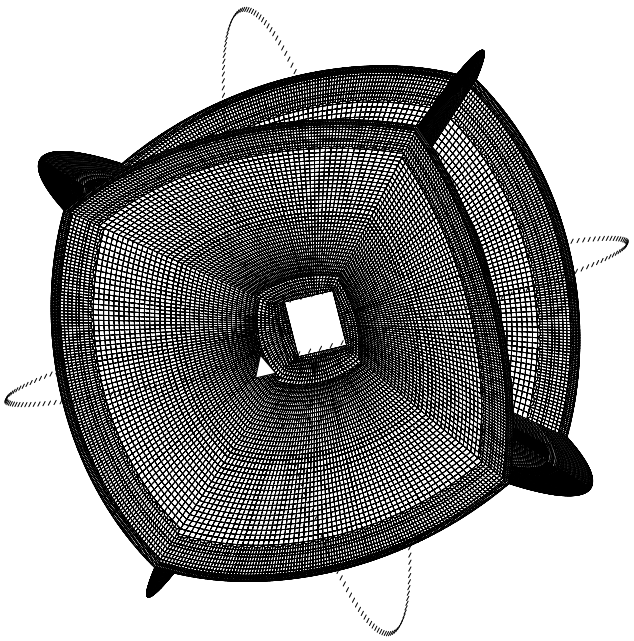

Figure 2: Mesh used for the simulations presented in this study. It honors all velocity discontinuities in the Earth model. The mesh is doubled in size three times with depth. Each of the six chunks has 240×240 elements at the surface of the Earth and 30×30 elements at the inner-core boundary. The triangle indicates the location of the epicenter of the earthquake, situated on the equator and the Greenwich meridian. Rings of receivers (seismic recording stations) with a 2-degree spacing along the equator and the Greenwich meridian are shown by the dashes.

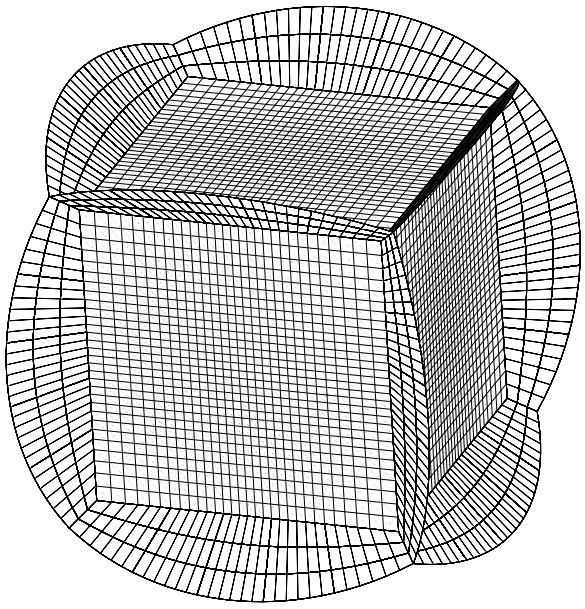

Figure 3: To avoid a mesh singularity associated with the Earth's center, we place a cube at the center of the solid inner core, following the idea introduced by [5]. This figure shows the actual mesh used. Note that there is a layer of three elements between the inner-core boundary and the central cube. Note also that element size within the central cube is not constant; this reflects a match-up with the angularly equidistant mesh at the inner-core boundary.

To avoid singularities of coordinates at the Earth's center, [5] introduced the idea of placing a cube around the center of the inner core. We make use of this idea in the present study. The mesh within this cube needs to match up with the cubed sphere mesh at the ICB, as shown in Figure 3.

3. THE SPECTRAL-ELEMENT METHOD

3.1 Equations of seismic wave motion

The elastic wave equation for the Earth's mantle, crust and solid inner-core may be written in the form

$$\rho\,\partial_t^2 \mathbf{s} = \boldsymbol{\nabla}\cdot\mathbf{T}, \tag{1}$$

where ρ denotes the 3-D distribution of density and $\mathbf{T}$ the stress tensor which is linearly related to the displacement gradient $\boldsymbol{\nabla}\mathbf{s}$ by Hooke's law, $\mathbf{T} = \mathbf{c} : \boldsymbol{\nabla}\mathbf{s}$. In its most general form, e.g., in a triclinic crystal, the fourth-order elastic tensor $\mathbf{c}$ has 21 independent components (e.g., [2]). Two types of boundary conditions must be considered: on the surface of the Earth the traction $\hat{\mathbf{n}}\cdot\mathbf{T}$, where $\hat{\mathbf{n}}$ denotes the unit outward normal on the free surface, vanishes, and on the CMB and the ICB (i.e., the fluid-solid boundaries) the normal component of velocity $\hat{\mathbf{n}}\cdot\mathbf{v}$ and the traction $\hat{\mathbf{n}}\cdot\mathbf{T}$ are continuous.

Spectral-element methods, like finite-element methods, are based upon an integral or 'weak' formulation of the problem. This formulation is obtained by taking the dot product of the momentum equation (1) with an arbitrary test-vector $\mathbf{w}$, integrating by parts and imposing the stress-free boundary condition. This gives

$$\begin{aligned}\int_{\mathrm{M}} \rho\,\mathbf{w}\cdot\partial_t^2\mathbf{s}\,\mathrm{d}^3\mathbf{r} = &- \int_{\mathrm{M}} \boldsymbol{\nabla}\mathbf{w} : \mathbf{T}\,\mathrm{d}^3\mathbf{r} + \mathbf{M} : \boldsymbol{\nabla}\mathbf{w}(\mathbf{r}_{\mathrm{s}})\,S(t) \\ &- \int_{\mathrm{CMB}} \mathbf{w}\cdot\mathbf{T}\cdot\hat{\mathbf{n}}\,\mathrm{d}^2\mathbf{r}. \end{aligned}\tag{2}$$

To correctly model interactions between the solid mantle and the fluid outer core, we need to impose the continuity of traction and of the normal velocity at the CMB. We implement the fluid-solid interactions based upon a simple and efficient domain decomposition method: in the mantle we impose the continuity of traction and in the fluid outer core we impose the continuity of normal velocity. The equations in the solid inner core of the Earth are similar to those presented above and are therefore not detailed here (since it is also a solid region in contact with the fluid outer core).

In the fluid outer core, the equation of motion can be written in terms of a scalar potential χ as

$$\kappa^{-1}\partial_t^2\chi = \boldsymbol{\nabla}\cdot(\rho^{-1}\boldsymbol{\nabla}\chi), \tag{3}$$

where κ is the bulk modulus of the fluid. That potential is related to pressure in the fluid by $p = -\partial_t\chi$. The weak form of this equation is obtained by multiplying it by a scalar test function w and integrating by parts. At the fluid-solid matching interfaces (the CMB and the ICB) we need to impose the continuity of normal velocity, therefore we replace the normal component of velocity $\hat{\mathbf{n}}\cdot\mathbf{v}$ in the integrals over the CMB and ICB with the normal component of velocity $\hat{\mathbf{n}}\cdot\partial_t\mathbf{s}$ in the mantle or inner core, which gives:

$$\begin{aligned}\int_{\mathrm{OC}} \kappa^{-1} w\partial_t^2\chi\,\mathrm{d}^3\mathbf{r} = &- \int_{\mathrm{OC}} \rho^{-1}\boldsymbol{\nabla}w\cdot\boldsymbol{\nabla}\chi\,\mathrm{d}^3\mathbf{r} \\ &- \int_{\mathrm{CMB}} w\,\hat{\mathbf{n}}\cdot\partial_t\mathbf{s}\,\mathrm{d}^2\mathbf{r} + \int_{\mathrm{ICB}} w\,\hat{\mathbf{n}}\cdot\partial_t\mathbf{s}\,\mathrm{d}^2\mathbf{r}. \end{aligned}\tag{4}$$

3.2 Interpolation, integration and discretization

To represent the displacement field on an element requires the introduction of grid points in each element. Typically, in a SEM it is optimal (in terms of the precision/cost ratio) to use Lagrange polynomials of degree 4 to 10 for the interpolation of functions [16]. This is much higher than the degree-1 or degree-2 approximations classically used in finite-element methods. The control points ξ are chosen to be the $l+1$ Gauss-Lobatto-Legendre points, which are the roots of $(1-\xi^2)P_l'(\xi) = 0$, where P_l' denotes the derivative of the Legendre polynomial of degree l (e.g., [3]). The reason for this choice is that it leads to an *exactly* diagonal mass matrix and therefore to fully explicit time schemes, which greatly simplifies the implementation of the method, in particular on a parallel computer. Functions f, such as the displacement field $\mathbf{s}$ and the test vector $\mathbf{w}$, are interpolated in terms of triple products of Lagrange polynomials. This choice of test vector makes the SEM a Galerkin method, because its basis functions are the same as those used to represent the displacement. The gradient of a function, $\boldsymbol{\nabla} f = \sum_{i=1}^{3} \hat{\mathbf{x}}_i \partial_i f$, evaluated at the Gauss-Lobatto-

Legendre point $\mathbf{x}(\xi_{\alpha'}, \eta_{\beta'}, \zeta_{\gamma'})$, may be written in the form

$$\boldsymbol{\nabla} f(\mathbf{x}(\xi_{\alpha'}, \eta_{\beta'}, \zeta_{\gamma'})) \approx \sum_{i=1}^{3} \hat{\mathbf{x}}_i \Bigg[\sum_{\alpha=0}^{n_\alpha} f^{\alpha\beta'\gamma'} \ell'_\alpha(\xi_{\alpha'}) \partial_i \xi + \sum_{\beta=0}^{n_\beta} f^{\alpha'\beta\gamma'} \ell'_\beta(\eta_{\beta'}) \partial_i \eta + \sum_{\gamma=0}^{n_\gamma} f^{\alpha'\beta'\gamma} \ell'_\gamma(\zeta_{\gamma'}) \partial_i \zeta \Bigg], \quad (5)$$

where the $\ell'(\xi)$ represent the derivatives of the Lagrange interpolants at the Gauss-Lobatto-Legendre points, and the $\partial_j \xi$ are the partial derivatives of the Jacobian transformation of the coordinate system to the $[-1,1]^3$ reference cube.

To solve the weak form of the equations of motion, numerical integrations over the elements need to be performed. In a spectral-element method, one uses the Gauss-Lobatto-Legendre integration rule:

$$\begin{aligned} \int_{\Omega_e} f(\mathbf{x}) \, \mathrm{d}^3\mathbf{x} &= \iiint_{-1}^{1} f(\mathbf{x}(\xi,\eta,\zeta)) \, J(\xi,\eta,\zeta) \, \mathrm{d}\xi \, \mathrm{d}\eta \, \mathrm{d}\zeta \\ &\approx \sum_{\alpha,\beta,\gamma=0}^{n_\alpha,n_\beta,n_\gamma} \omega_\alpha \omega_\beta \omega_\gamma f^{\alpha\beta\gamma} J^{\alpha\beta\gamma}, \end{aligned} \quad (6)$$

where the ω_α denote the weights associated with the Gauss-Lobatto-Legendre quadrature (e.g., [3]), and J is the Jacobian of the transformation of the coordinate system to the $[-1,1]^3$ reference cube.

The term on the left hand side of the weak form of the equation of motion (2) is traditionally called the *mass matrix* in finite-element modeling. At the elemental level, this integration may be written as

$$\begin{aligned} &\int_{\Omega_e} \rho \, \mathbf{w} \cdot \partial_t^2 \mathbf{s} \, \mathrm{d}^3\mathbf{x} \\ &\quad = \iiint_{-1}^{1} \rho(\mathbf{x}(\boldsymbol{\xi})) \, \mathbf{w}(\mathbf{x}(\boldsymbol{\xi})) \cdot \partial_t^2 \mathbf{s}(\mathbf{x}(\boldsymbol{\xi}), t) \, J(\boldsymbol{\xi}) \, \mathrm{d}^3\boldsymbol{\xi} \\ &\quad \approx \sum_{\alpha,\beta,\gamma=0}^{n_\alpha,n_\beta,n_\gamma} \omega_\alpha \omega_\beta \omega_\gamma J^{\alpha\beta\gamma} \rho^{\alpha\beta\gamma} \sum_{i=1}^{3} w_i^{\alpha\beta\gamma} \ddot{s}_i^{\alpha\beta\gamma}(t). \end{aligned} \quad (7)$$

By independently setting factors of $w_1^{\alpha\beta\gamma}$, $w_2^{\alpha\beta\gamma}$ and $w_3^{\alpha\beta\gamma}$ equal to zero, since the weak formulation (2) must hold for *any* test vector $\mathbf{w}$, we obtain an equation for each component of acceleration $\ddot{s}_i^{\alpha\beta\gamma}(t)$ at grid point $(\xi_\alpha, \xi_\beta, \xi_\gamma)$, that we can subsequently march explicitely in time. The remarkable property of equation (7) is that the value of acceleration at each point of a given element, $\ddot{s}_i^{\alpha\beta\gamma}(t)$, is simply multiplied by the factor $\omega_\alpha \omega_\beta \omega_\gamma \rho^{\alpha\beta\gamma} J^{\alpha\beta\gamma}$, i.e., as mentioned earlier, the elemental mass matrix is exactly diagonal. This has a very important implication in practice, since it greatly simplifies the message-passing implementation of the SEM algorithm. Note also that in this respect the SEM significantly differs from more traditional finite-element methods, in which a sparse (i.e., non diagonal) system would be obtained.

The next integral that needs to be evaluated is the *stiffness matrix* (the first term of the right-hand side of equation (2)). We find

$$\begin{aligned} \int_{\Omega_e} \boldsymbol{\nabla}\mathbf{w} : \mathbf{T} \, \mathrm{d}^3\mathbf{x} \quad \approx \\ \sum_{\alpha,\beta,\gamma=0}^{n_\alpha,n_\beta,n_\gamma} \sum_{i=1}^{3} w_i^{\alpha\beta\gamma} \Bigg[\omega_\beta \omega_\gamma \sum_{\alpha'=0}^{n_{\alpha'}} \omega_{\alpha'} J_e^{\alpha'\beta\gamma} F_{i1}^{\alpha'\beta\gamma} \ell'_\alpha(\xi_{\alpha'}) \\ + \omega_\alpha \omega_\gamma \sum_{\beta'=0}^{n_{\beta'}} \omega_{\beta'} J_e^{\alpha\beta'\gamma} F_{i2}^{\alpha\beta'\gamma} \ell'_\beta(\eta_{\beta'}) \\ + \omega_\alpha \omega_\beta \sum_{\gamma'=0}^{n_{\gamma'}} \omega_{\gamma'} J_e^{\alpha\beta\gamma'} F_{i3}^{\alpha\beta\gamma'} \ell'_\gamma(\zeta_{\gamma'}) \Bigg], \end{aligned} \quad (8)$$

where $F_{ik} = \sum_{j=1}^{3} T_{ij} \, \partial_j \xi_k$. The value of the stress tensor $\mathbf{T}$ is determined by Hooke's law, $\mathbf{T} = \mathbf{c} : \boldsymbol{\nabla}\mathbf{s}$. This calculation requires knowledge of the gradient of displacement $\boldsymbol{\nabla}\mathbf{s}$ at the Gauss-Lobatto-Legendre integration points, which is given by:

$$\begin{aligned} \partial_i s_j(\mathbf{x}(\xi_\alpha, \eta_\beta, \zeta_\gamma), t) = \\ \left[\sum_{\sigma=0}^{n_\sigma} s_j^{\sigma\beta\gamma}(t) \ell'_\sigma(\xi_\alpha) \right] \partial_i \xi(\xi_\alpha, \eta_\beta, \zeta_\gamma) \\ + \left[\sum_{\sigma=0}^{n_\sigma} s_j^{\alpha\sigma\gamma}(t) \ell'_\sigma(\eta_\beta) \right] \partial_i \eta(\xi_\alpha, \eta_\beta, \zeta_\gamma) \\ + \left[\sum_{\sigma=0}^{n_\sigma} s_j^{\alpha\beta\sigma}(t) \ell'_\sigma(\zeta_\gamma) \right] \partial_i \zeta(\xi_\alpha, \eta_\beta, \zeta_\gamma). \end{aligned} \quad (9)$$

The remaining volume and surface integrals in (2) and (4) are identical in form to other integrals already discussed in this section.

3.3 Assembly of the system and time marching

In each spectral element, functions are sampled at the Gauss-Lobatto-Legendre points. Grid points that lie on the sides, edges, or corners of an element are shared amongst neighbors. Therefore, as in a classical finite-element method, we need to distinguish the *local mesh* of grid points that define an element from the *global mesh* of all the grid points in the model, many of which are shared amongst several spectral elements. Note that there are three unknowns (or 'degrees of freedom' in finite-element parlance) per grid point in the solid regions of the model (the three components of the displacement vector), but only one degree of freedom in the fluid outer core (the generalized scalar potential χ). The contributions to the degrees of freedom (i.e., the internal forces computed separately) from all the elements that share a common global grid point need to be summed to obtain the right global internal forces. In a traditional finite-element method this is referred to as *assembling* the system. This assembly stage is a costly part of the calculation on parallel computers, because information from individual elements needs to be shared with neighboring elements. In a SEM, this is the only operation that involves communications between distinct CPUs (implemented based upon MPI in practice).

To take full advantage of the fact that the global mass matrix is exactly diagonal, time discretization of the resulting global second-order ordinary differential equation obtained after assembling the system is achieved based upon an explicit second-order finite-difference scheme. Such a scheme,

which is a particular case of the general Newmark scheme for second-order hyperbolic systems [9], is conditionally stable, and the Courant stability condition is governed by the maximum value of the ratio between the pressure wave velocity and the size of the grid spacing.

4. PARALLEL IMPLEMENTATION USING MPI ON A BEOWULF

We implement the method on a cluster of PCs using message passing (MPI). In our SEM, since the mass matrix is exactly diagonal by construction, the PCs spend most of their time doing computations, and communications represent only a small fraction of the time of simulation. Therefore, this is an optimal situation for a parallel implementation, and clusters of PCs are ideal for this application in spite of the high latency of the network connecting them.

The SEM calculations are performed on a Beowulf in the Seismological Laboratory at Caltech. This machine consists of 76 dual-processor PCs with 1 Gigabyte of memory each. The PCs are connected using standard 100-Mbits Ethernet. The simulations are distributed over 151 processors. Each of the six chunks that constitute the globe is subdivided amongst 25 processors (corresponding to 25 mesh slices), and the cube at the center of the inner core uses one separate processor. Figure 4 shows how the slices are designed in the cubed-sphere mesh. Note that inside each of the six chunks the mesh of slices is derived from a regular Cartesian topology. However, the message passing topology must be different between chunks: each corner of each chunk is shared between three rather than two or four slices. This complicates the message-passing implementation. We solve the problem using a three-step sequence of messages: we first assemble the contributions between slices inside each chunk; then between slices located on the edges of different chunks, excluding the corners of valence 3; then in a last step we assemble these corners separately.

The mesh shown in Figures 2 and 3 contains a total of approximately 2.6 million spectral elements. In each spectral element we use a polynomial degree $N = 4$ for the expansion of the Lagrange interpolants at the Gauss-Lobatto-Legendre points, which means each spectral element contains $(N + 1)^3 = 125$ points, and the total global system of ordinary differential equations, counting common points on the edges of the elements only once, contains 179 million points (i.e., approximately 539 million degrees of freedom since we solve for the three components of displacement at each grid point in the solid regions). After division of the mesh into slices, each processor is responsible for 17,000 elements. With a polynomial degree $N = 4$, this corresponds to roughly 1.1 million grid points per processor.

The central cube in the inner core, shown in Figure 3, poses yet another difficulty from a message-passing point of view. Since it is handled by a separate processor, and since it shares grid points with all the other slices, a separate communication pattern has to be implemented based upon a master-slave programming philosophy: all the slices send their contributions (the internal forces computed locally) to the central cube, which acts as a master, collecting and summing them, and then sending the result back to the slices, which act as slaves. The number of elements in the central cube is smaller than in any of the slices, which ensures that load balancing of the application is unaffected.

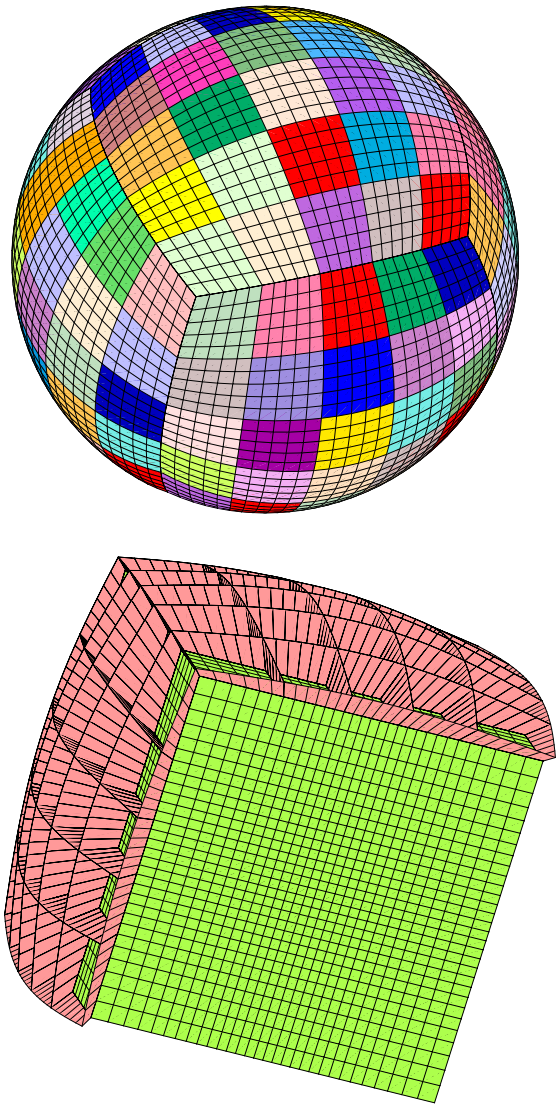

Figure 4: In the parallel MPI implementation, each of the six chunks that makes up the cubed sphere is subdivided in terms of 25 slices of elements (top). Each of these slices resides on a single CPU. The central cube (bottom) is handled by one extra processor, such that the entire calculation involves 151 CPUs. The results on the edges of a slice need to be communicated to all its neighbors. Note that the communication patterns are different for slices inside a chunk, on the edges of a chunk, and on the corners of a chunk. The MPI communication pattern is particularly difficult for the central cube, which is handled by a separate processor that needs to communicate with all the other processors, because every slice of the mesh touches it (here some slices have been removed for clarity). One needs to use a master/slave programming methodology in order to avoid communication patterns that could deadlock.

5. THE GREAT BOLIVIAN EARTHQUAKE OF JUNE 9, 1994

We benchmark the SEM against an independent reference solution for the anisotropic reference Earth velocity and density model PREM. We use the mesh and source-receivers (i.e., epicenter of the earthquake and seismic recording stations) geometry shown in Figure 2. For simplicity, the epicenter of the earthquake is located on the equator and the Greenwich meridian. Note that because the PREM velocity model is spherically symmetric, this is strictly equivalent to using the real location of the event in Bolivia. Seismic stations record ground displacement along the equator and the Greenwich meridian at 2-degree intervals. For comparison and validation, we use a classical independent reference solution computed based upon a quasi-analytical normal-mode summation technique (e.g., [6]). Note that the normal-mode method is very accurate, but limited to spherically-symmetric models (i.e., to 3-D simulations in 1-D radial structures such as PREM), whereas our SEM can handle fully 3-D velocity models.

We simulate a large and very deep earthquake of magnitude $M_w = 8.2$ that occured in Bolivia on June 9, 1994, at a depth of 647 km. This earthquake is one of the largest deep events ever recorded, and has therefore generated a lot of attention in the seismological community. The event has significant energy down to a period of about 15 seconds (i.e., for frequencies below 67 mHz). We also include the effect of attenuation (i.e., anelastic behavior) in this simulation; the reader is referred to [10] for more details on how attenuation is implemented in the SEM (it is not straightforward to implement attenuation in time-domain methods, because in principle determining the current state of an anelastic medium requires a convolution with all the past history of that medium, which is of course numerically impossible).

In Figure 5 we represent an image of the seismic waves at two different times, showing how the pressure, shear and surface waves propagate across the Earth. In Figure 6 we compare normal-mode and SEM synthetic seismograms (i.e., the displacement of the Earth's surface with time at a given location) at a distance of 5 degrees south of the epicenter in Bolivia. We find excellent agreement between the two results. In particular, the pressure (P) wave and shear (S) wave arrivals, as well as the strong near-field term linking them, are accurately modeled, and the static offset of 6.6 mm on the vertical component of displacement and 7.3 mm on the North-South component is also well recovered. This so-called static offset corresponds to a permanent displacement of the surface of the Earth around the epicenter, due to the very large magnitude of the earthquake (this permanent displacement is also very clear on the second image of Figure 5). Note also the distinct arrival called ScS on this component at 800 seconds and the arrival called sScS at 1080 seconds, which are perfectly reproduced. These so-called ScS phases are waves that travel down to the core-mantle boundary at a depth of 2891 km, where they are reflected because of the fluid-solid impedance contrast, and then travel back to the surface.

Next, we check the results of our simulation at a seismic station located in Pasadena, California, at an epicentral distance of 68°. In Figure 7 we compare our SEM synthetic calculation for the vertical component of velocity to the real data recorded during the actual event. The signals

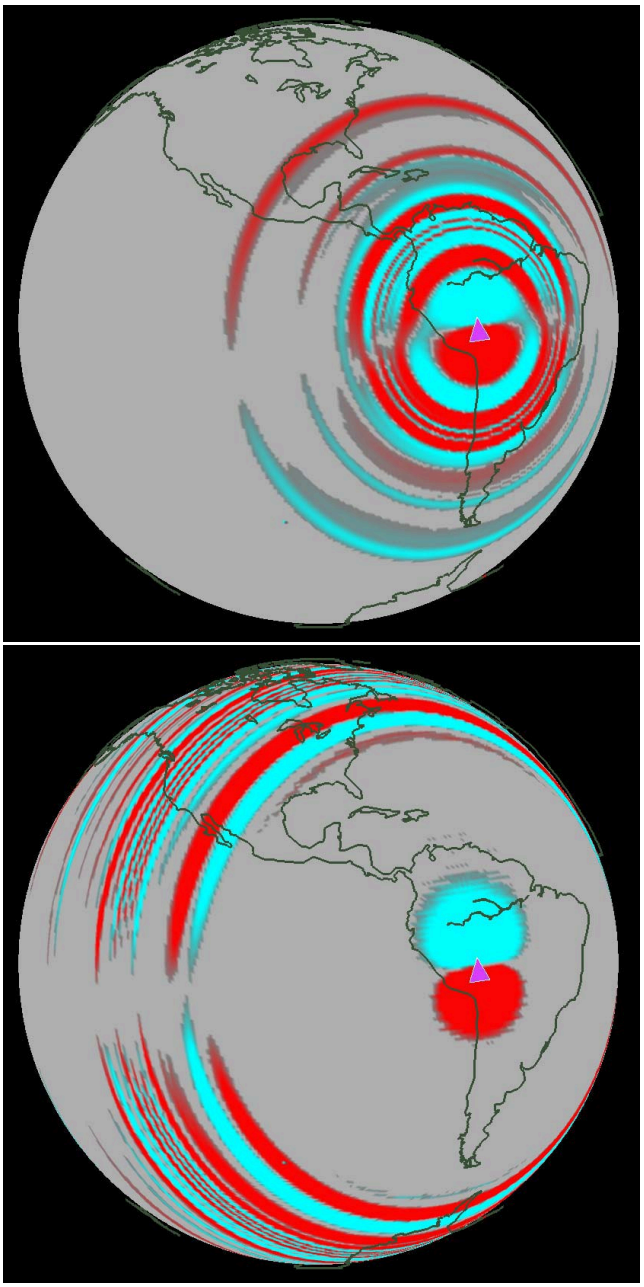

Figure 5: Movie of the propagation of seismic waves in the Earth during the large magnitude 8.2 Bolivia earthquake of June 9, 1994. The waves travel all across the globe. They can be seen propagating across the United States for instance. The earthquake is so large that it produces a permanent displacement of the surface of the Earth of several millimeters (1/4th of an inch) around the epicenter in Bolivia. Note that this effect extends as far North as the Amazon river.

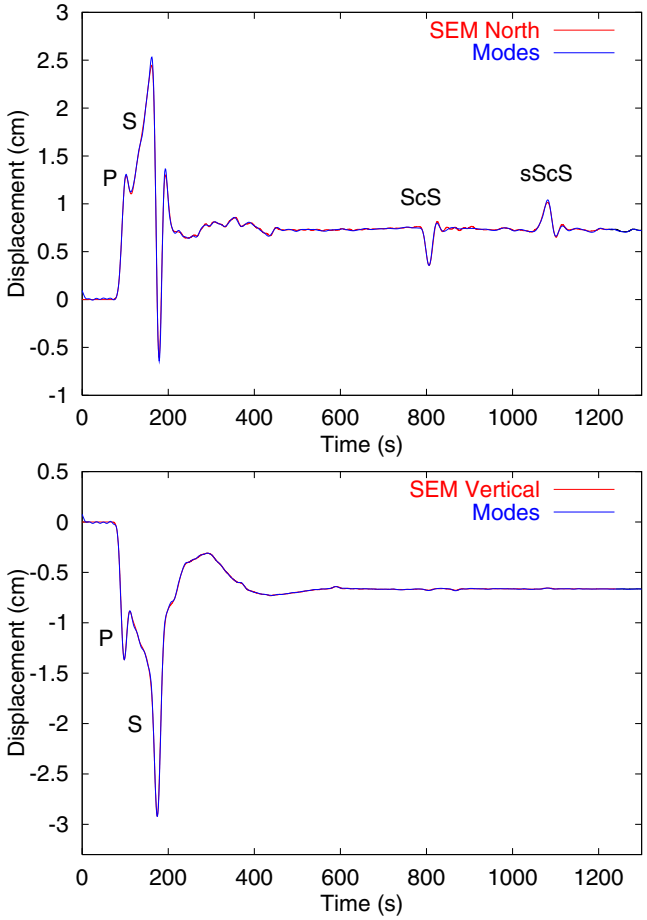

Figure 6: SEM (red) and quasi-analytical normal-mode reference (blue) synthetic seismograms for the great magnitude 8.2 Bolivia earthquake of June 9, 1994 recorded 5 degrees south of the epicenter. The depth of the earthquake is 647 km. Anisotropy and attenuation are both included in this simulation. Top: North-South component of displacement of the Earth's surface, Bottom: vertical component. Note the strong near-field term linking the pressure (P) and shear (S) waves, the large 6.6 mm and 7.3 mm static offsets observed on the two components, as well as the strong ScS and sScS shear waves reflected off the fluid outer core of the Earth.

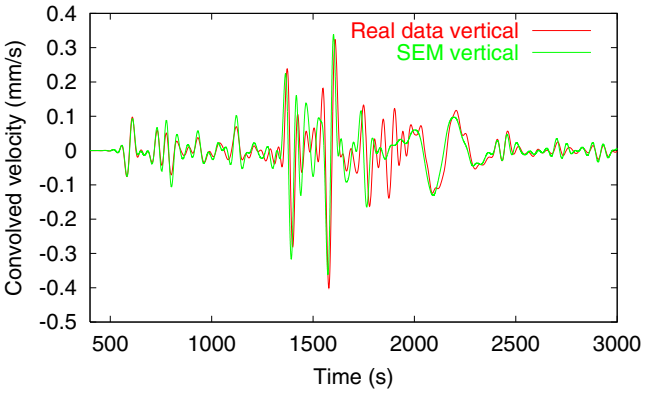

Figure 7: Comparison between our SEM synthetic seismograms for the anelastic, anisotropic reference Earth model PREM, and real seismic data recorded in Pasadena, California, during the actual June 9, 1994, Bolivia earthquake. The vertical component of the velocity vector is shown. The agreement obtained is very good, considering that our SEM results do not include the full complexity due to 3-D model heterogeneity, in particular in the crust and the mantle of the Earth.

recorded correspond to the waves that travel across Southern California on the movie of Figure 5. Both records have been lowpass-filtered with the same six-pole two-pass Butterworth filter with a corner period of 40 seconds (i.e., a corner frequency of 25 mHz), and our synthetics have been convolved with the instrument response of the seismic station. The agreement is quite satisfactory, keeping in mind that our synthetics are based upon the spherically-symmetric reference model PREM and therefore do not include more complex effects due to 3-D model heterogeneity. We are currently in the process of taking such 3-D velocity models into account in our SEM.

To illustrate that our implementation of the inner core with the central cube of Figure 3 is correct, we show in Figure 8 a close-up of the so-called PKP arrivals on the vertical component of the displacement vector around the antipode of the epicenter of the earthquake. The PKP phases are waves that have traveled as pressure waves both in the mantle and in the outer core of the Earth. These phases have three branches: PKP(AB) and PKP(BC), which travel in the fluid outer core but not in the solid inner core, and PKP(DF), which goes into the inner core. The PKP(DF) waveform is very sensitive to the very slow shear-wave velocity of about 3.6 km.s^{-1} in the inner core. If this unusually low velocity is not correctly represented numerically, the PKP(DF) waveform changes considerably. This poses a challenge, because if the mesh is not fine enough the very slow shear-wave velocity is not sampled by enough points per seismic wavelength, and as a result strong numerical noise is generated.

In our results, the PKP(AB) and PKP(BC) outer core branches as well as the PKP(DF) inner core branch are all very accurately modeled. The PKP(DF) arrival travels through the small cube at the center of the inner core which is handled by one processor that needs to interact with all the other processors in the parallel implementation

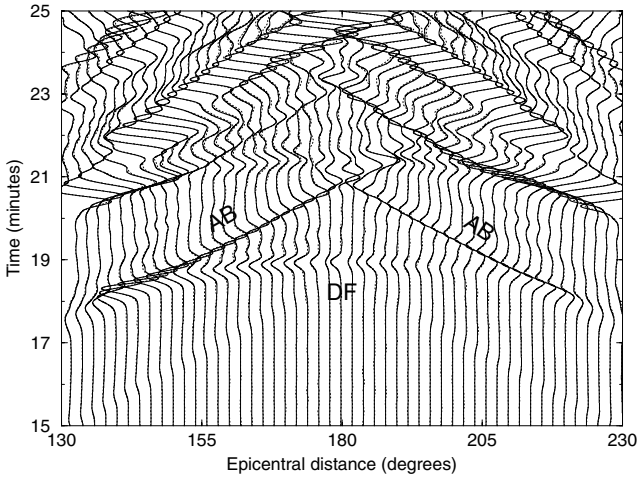

Figure 8: Record section comparison of outer-core and inner-core PKP pressure waves calculated for the anelastic, anisotropic Earth velocity model PREM based upon the SEM (solid lines) and an independent quasi-analytical normal-mode reference calculation (dotted lines) between 130° and 230°. At each epicentral distance we plot both the SEM and the normal-mode solution. All PKP arrivals, including PKP(DF), which has traveled through the central cube in the mesh (Figure 4), are well reproduced. This validates the master/slave parallel programming methodology that is used to implement the inner core, as illustrated in Figure 4. It also demonstrates that we can correctly handle the unusually low value of shear-wave velocity in the Earth's inner core.

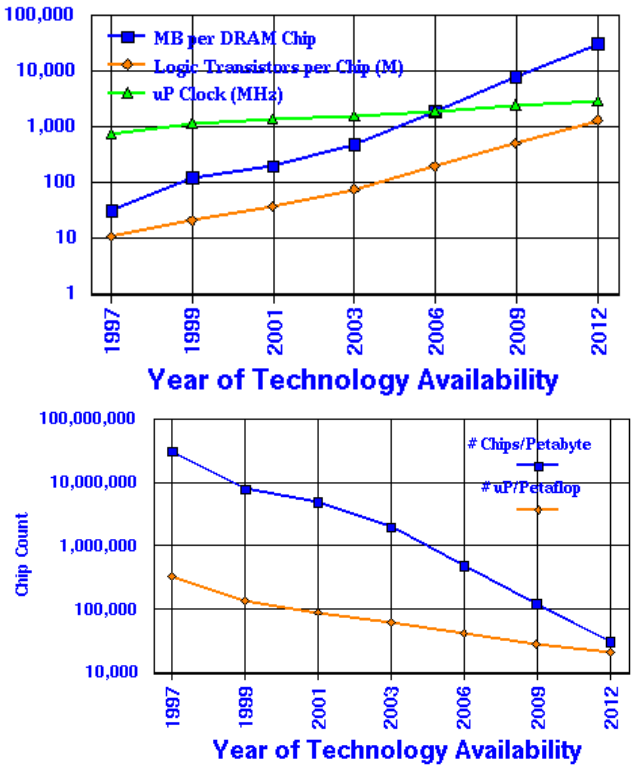

Figure 9: Projected evolution until 2012 of microprocessor clock speed, memory capacity and number of transistors per chip, showing that around 2010 the scientific community might have access to Petaflop machines consisting typically of several tens of thousands of chips. Courtesy Dr. Tom Sterling, Caltech.

of the method (Figure 4), therefore this result validates all of our MPI implementation.

6. CONCLUSIONS AND PERSPECTIVES

We have developed and implemented a parallel MPI spectral element method (SEM) for the simulation of seismic wave propagation resulting from large earthquakes at the scale of the full 3-D Earth. The method has been benchmarked against a classical quasi-analytical normal-mode reference solution for the spherically symmetric Earth velocity model PREM. Excellent agreement has been obtained.

The calculations presented in this paper required 151 processors and 50 Gb of memory and used tens of hours of CPU time. These requirements may seem large, but within ten years, computers reaching 1000 teraflops (1 petaflop) will become available, and the calculations presented in this study will be performed routinely in a matter of seconds or minutes. For instance, Figure 9 (courtesy of Dr. Tom Sterling from his Supercomputing'2000 presentation) shows the expected evolution of microprocessor clock speed, memory capacity and number of transistors per chip. One can see that according to these projections, around 2010 the scientific community might have access to Petaflop machines consisting typically of several tens of thousands of chips. This is in agreement with a linear extrapolation (in a semilog scale) until 2010 of the evolution of the speed of the fastest

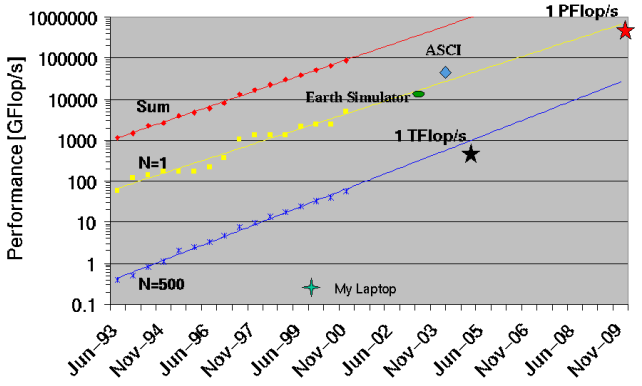

Figure 10: Linear extrapolation in a semilog scale (yellow curve) of the projected evolution of the speed of the fastest computer of the TOP500 list (*www.top500.org*) until 2010, showing that the fastest computers might reach the petaflop range 10 years from now. Courtesy Dr. Tom Sterling, Caltech.

computer of the TOP500 list (*www.top500.org*). Figure 10 (also courtesy of Dr. Tom Sterling from his Supercomputing'2000 presentation) shows that the world's fastest computers might reach the petaflop range 10 years from now. Let us mention that the ASCI and the Blue Gene projects already plan to reach 30 to 100 Teraflops around 2003-2005.

We are also currently in the process of adding more complexity to our simulations in terms of the Earth model used, i.e., fully 3-D mantle models with lateral variations of density and pressure and shear-wave velocities, ellipticity and surface topography of the Earth, as well as gravity and rotation (Coriolis force) which have an effect on long-period surface waves.

7. ACKNOWLEDGMENTS

The authors thank Luis Rivera, Philip and Rachel Abercrombie, Roland Martin, Tom Sterling, Emmanuel Chaljub, Yann Capdeville, Jan Lindheim, Ewing Lusk, Hans-Peter Bunge and Paul F. Fischer for fruitful discussions and comments. This material is based in part upon work supported by the National Science Foundation under Grant No. 0003716. This is Caltech GPS contribution No. 8823.

8. REFERENCES

[1] C. Bernardi, N. Debit, and Y. Maday. Coupling finite element and spectral methods: first results. *Mathematics of Computation*, 54:21–39, 1990.

[2] L. Brillouin. *Tensors in Mechanics and Elasticity.* Academic Press, New York, 3rd edition, 1964.

[3] C. Canuto, M. Y. Hussaini, A. Quarteroni, and T. A. Zang. *Spectral methods in fluid dynamics.* Springer-Verlag, New York, 1988.

[4] Y. Capdeville. *Méthode couplée éléments spectraux - solution modale pour la propagation d'ondes dans la Terre à l'échelle globale (A coupled method using spectral elements and normal modes for global wave propagation in the Earth).* PhD thesis, Université Paris VII Denis Diderot, Paris, France, 2000.

[5] E. Chaljub. *Modélisation numérique de la propagation d'ondes sismiques en géométrie sphérique: application à la sismologie globale (Numerical modeling of the propagation of seismic waves in spherical geometry: applications to global seismology).* PhD thesis, Université Paris VII Denis Diderot, Paris, France, 2000.

[6] F. A. Dahlen and J. Tromp. *Theoretical Global Seismology.* Princeton University Press, Princeton, 1998.

[7] A. M. Dziewonski and D. L. Anderson. Preliminary reference Earth model. *Phys. Earth Planet. Inter.*, 25:297–356, 1981.

[8] E. Faccioli, F. Maggio, R. Paolucci, and A. Quarteroni. 2D and 3D elastic wave propagation by a pseudo-spectral domain decomposition method. *J. Seismol.*, 1:237–251, 1997.

[9] T. J. R. Hughes. *The finite element method, linear static and dynamic finite element analysis.* Prentice-Hall International, Englewood Cliffs, NJ, 1987.

[10] D. Komatitsch and J. Tromp. Introduction to the spectral-element method for 3-D seismic wave propagation. *Geophys. J. Int.*, 139:806–822, 1999.

[11] D. Komatitsch and J. P. Vilotte. The Spectral Element method: an efficient tool to simulate the seismic response of 2D and 3D geological structures. *Bull. Seis. Soc. Am.*, 88(2):368–392, 1998.

[12] A. T. Patera. A spectral element method for fluid dynamics: laminar flow in a channel expansion. *J. Comput. Phys.*, 54:468–488, 1984.

[13] E. Priolo, J. M. Carcione, and G. Seriani. Numerical simulation of interface waves by high-order spectral modeling techniques. *J. Acoust. Soc. Am.*, 95(2):681–693, 1994.

[14] C. Ronchi, R. Ianoco, and P. S. Paolucci. The "Cubed Sphere": a new method for the solution of partial differential equations in spherical geometry. *J. Comput. Phys.*, 124:93–114, 1996.

[15] R. Sadourny. Conservative finite-difference approximations of the primitive equations on quasi-uniform spherical grids. *Monthly Weather Review*, 100:136–144, 1972.

[16] G. Seriani and E. Priolo. A spectral element method for acoustic wave simulation in heterogeneous media. *Finite Elements in Analysis and Design*, 16:337–348, 1994.

[17] M. Taylor, J. Tribbia, and M. Iskandarani. The spectral element method for the shallow water equation on the sphere. *J. Comput. Phys.*, 130:92–108, 1997.